Journal of Colloid and Interface Science 474 (2016) 179–189

Contents lists available at ScienceDirect

Journal of Colloid and Interface Science

journal homepage: www.elsevier.com/locate/jcis

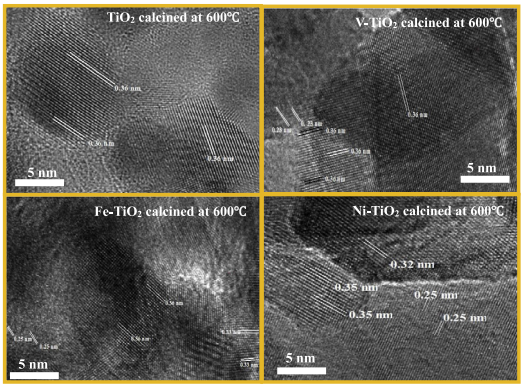
Investigation of the influence of vanadium, iron and nickel dopants on the morphology, and crystal structure and photocatalytic properties of titanium dioxide based nanopowders

Godlisten N. Shao [a,b], Sun-Jeong Jeon [a], M. Salman Haider [c,d], Nadir Abbass [a], Hee Taik Kim [a,*]

[a] Department of Chemical Engineering, Hanyang University, 1271 Sa 3-dong, Sangnok-gu, Ansan-si, Gyeonggi-do 426-791, Republic of Korea
[b] Department of Chemistry, Mkwawa College, University of Dar es Salaam, Iringa, United Republic of Tanzania
[c] Department of Civil and Evironmental Engineering, Hanyang University, 1271 Sa 3-dong, Sangnok-gu, Ansan-si, Gyeonggi-do 426-791, Republic of Korea
[d] Department of Chemical Engineering, University of Gujrat, HH Campus, Punjab, Pakistan

GRAPHICAL ABSTRACT

High resolution TEM of pure and doped titania photocatalysts.



ARTICLE INFO

Article history:
Received 31 January 2016
Revised 18 April 2016
Accepted 19 April 2016
Available online 22 April 2016

Keywords:
Sol-gel process
$TiOCl_2$
Calcination
Heterogeneous photocatalysis

ABSTRACT

Photoactive V, Fe and Ni doped TiO_2 (M-TiO_2) nanopowders were synthesized by a modified two-step sol-gel process in the absence of additives. Titanium oxychloride, which is a rarely-used TiO_2 precursor was used to yield M-TiO_2 photocatalysts with preferential photochemical performance in the presence of natural solar irradiation. The obtained samples were calcined at different calcination temperatures ranging from 450 to 800 °C to evaluate the influence of the sintering on the physicochemical properties. The properties of the obtained samples were examined by XRF, XRD, Raman spectroscopy, UV–visible DRS, XPS, nitrogen gas physisorption studies, SEM-EDAX and HRTEM analyses. Structural characterization of the samples revealed the incorporation of these transition metal element into TiO_2. It was also depicted that the morphology, crystal structure, optical and photochemical properties of the obtained samples were largely dependent on the calcination temperature and the type of dopant used during the preparation process. The photochemical performance of the samples was investigated in the photodegradation of methylene blue in the presence of natural sunlight. The experimental results indicated that the VT600 sample possessed the highest activity due to its superior properties. This study provides a systematic preparation and selection of the precursor, dopant and calcination temperature that are suitable for

* Corresponding author.
E-mail addresses: khtaik@yahoo.com, khtaik@hanyang.ac.kr (H.T. Kim).

http://dx.doi.org/10.1016/j.jcis.2016.04.024
0021-9797/© 2016 Elsevier Inc. All rights reserved.

the formation of TiO_2-based heterogeneous photocatalysts with appealing morphology, crystal structure, optical and photochemical properties for myriad of applications.

© 2016 Elsevier Inc. All rights reserved.

1. Introduction

Metal oxides semiconductors such as TiO_2, ZnO, WO_3, In_2O_3 and SnO_2 have attracted much attention due to their wide applications in solar cells, heterogeneous photocatalysis, hydrogen gas production through photocatalytic water splitting and sensor technologies. Of the metal oxide semiconductors that have been investigated, TiO_2-based materials have shown remarkable performances due to their unique thermal, electrochemical and optical properties [1–8]. This has significantly prompted many researchers to design versatile preparation approaches to facilitate large-scale production of TiO_2-based materials [9–11]. TiO_2 occurs in three different polymorphic structures: anatase, brookite or rutile phases. These polymorphs can be prepared readily from TiO_2 sources and typically the metastable anatase and brookite transforms into the thermodynamically stable rutile upon calcination at high temperatures [12–15].

The wide band gap of TiO_2 (E_g = ~3.0–3.3 eV) and the rapid recombination of its photogenerated electron–hole pairs hamper the performance of TiO_2 in some applications especially in those that require visible light excitation [13–17]. Various research investigations [13–19] have proposed that TiO_2 material with a mixture of titania phases exhibits improved quantum efficiency compared to single phase material. Thus, the photochemical performance of the former is thought to be superior to that of the latter. So far, various preparation methods have been suggested that allow for the preparation of metal oxide semiconductors with promising properties for numerous applications. These include co-precipitation, ball milling, spray pyrolysis, hydrothermal, sol-gel, chemical vapor deposition techniques and others [7,8,20–25]. However, the sol-gel process has undoubtedly attracted much attention due to its simplicity, cost-effectiveness and ability to form homogeneous and pure final products at ambient conditions [12,18]. Therefore, the formulation of simplified and convenient sol-gel synthetic routes to prepare metal oxide semiconductors from less expensive precursors will considerably enhance the large-scale production and commercialization of these potential materials.

Meanwhile, there are promising strategies than can be used to extend the optical absorption of TiO_2 into the visible region while simultaneously reducing the recombination behavior of the photogenerated charge carriers during photocatalysis. These include non-metal doping (N, S, C or F); noble metal and transition metal deposition (Au, Ag, Fe, Co, Pt, V or Ni); and the formation of oxygen-rich TiO_2 [8,16,17,20–26]. TiO_2 photocatalysts doped with transition metals and rare earth elements such as Cu, W, Ce, Ni, Eu, La, Nb, Y, V and Fe have been widely investigated. Various studies [17,26,27] have shown that transition metal doped TiO_2-based materials exhibit high photocatalytic performance under visible light irradiation. It has also been deduced that the presence of these species can affect phase transition, morphology and optical properties of the yielded materials. Nevertheless, in most reports, commercial TiO_2 or highly pure metal alkoxide precursors such as tetrabutyl orthotitanate or titanium isopropoxide are utilized as titania sources. Additionally, additives such as tri-block copolymer, polyethylene glycol and cetyltrimethylammonium bromide are used to act as structure-directing agents [21,24,27,28]. This causes the production of TiO_2 based materials to be more expensive and tedious; therefore, the large-scale production and commercialization of heterogeneous photocatalysts is adversely hampered.

In our previous study [20] we found that doping TiO_2 with vanadium has three substantial effects on the mesostructure of the obtained photocatalysts: (1) it reduces the aggregation behavior of the primary particles of the obtained photocatalysts; (2) it facilitates the formation of photocatalysts with a mixture of brookite, anatase and rutile phases; and moreover, (3) it remarkably extends the optical absorption of the obtained products to the visible region. These three outcomes are crucial for the production of final products that possess enhanced photocatalytic performance in the presence of natural solar irradiation. Therefore, it is prudent to carry out a study to compare the morphology, crystal structure, optical properties and photocatalytic performance of Fe, V and Ni doped TiO_2 photocatalysts that are obtained from simple and convenient preparation methods. The ionic radii of V^{5+} (0.063 nm), Fe^{3+} (0.065 nm) and Ni^{2+} (0.069 nm) are very close to that of Ti^{4+} (0.068 nm) and therefore, they can easily be doped into TiO_2 to yield visible light-active (VLA) materials with desirable properties for heterogeneous photocatalysis [29].

The present study compares the morphology, crystal structure and photocatalytic properties of sol-gel based V, Fe and Ni doped TiO_2 photocatalysts in the absence of additives. A controllable, reproducible and cost-effective sol-gel process was used to synthesize photoactive V, Fe and Ni doped TiO_2 heterogeneous photocatalysts. The sol-gel process proposed in the present study involves peptization of the preformed TiO_2 gel using an acidic solution of metal ions precursors which allows the formation of porous products with a homogeneous dispersion of primary particles in the absence of additives. The photochemical performance of the formed photocatalysts was evaluated in the degradation of methylene in the presence of natural solar irradiation. To the best of our knowledge, only a few reports [24,26] have investigated the influence of transition metals on the mesostructure of TiO_2-based materials. None of these has provided a systematic comparison using the preparation method and titania precursor proposed in the present study. Moreover, the photochemical performances of the obtained photocatalysts were evaluated in the photodecolorization of a methylene blue solution in the presence of solar irradiation to substantiate their practical reliability in degrading non-biodegradable toxic organic contaminants.

2. Experimental part

2.1. Materials

All of the chemical reagents used in this study were purchased from commercial sources and used without further purification. $TiOCl_2$ (25 wt%) was purchased from Kukdong Chemicals Co. Ltd, South Korea while ammonium hydroxide solution (28%) was bought from Dae-Jung Chemical and Metal Co. Ltd, South Korea. Iron (III) nitrate nonahydrate (98+%), methylene blue hydrate and HNO_3 (60%) were acquired from Sigma-Aldrich. Vanadium pentaoxide (99%) was procured from Junsei Chemical Co. Ltd, Japan and nickel (II) nitrate hexahydrate (98%) was acquired from Duksan Pharmaceutical Co. Ltd, South Korea.

2.2. Synthesis process

Photoactive V, Fe or Ni doped TiO_2 photocatalysts were synthesized through two-step modified sol-gel synthetic approach in the

absence of surfactants. We followed the experimental procedures described in our previous report with some modifications [20]. Initially, 0.3 mmol of V_2O_5 was added into a beaker containing 60 mL of 0.02 M nitric acid and the solution was stirred for 2 h (**Solution A**). Into another separate beaker containing 60 mL of de-ionized (DI) water, 10 mL of $TiOCl_2$ was added and the obtained solution was stirred for 1 h (**solution B**). S**olution B** was then gelated through the drop-wise addition of the ammonium hydroxide solution. The two-step process was attained by peptizing the gel obtained from **solution B** using **solution A** and then stirred vigorously for 2 h (**solution C**). The pH of **solution C** was adjusted to 6 in order to obtain a slurry. The temperature of the slurry was raised from room temperature to 80 °C and aged under constant stirring for 6 h. After 6 h the temperature of the slurry was lowered to room temperature and the product was recovered by vacuum filtration and dried at 100 °C for 6 h. The same experimental procedures were followed using either 0.3 mmol of Fe $(NO_3)_3{\cdot}9H_2O$ or 0.3 mmol of Ni $(NO_3){\cdot}6H_2O$ to yield Fe-TiO_2 and Ni-TiO_2 samples, respectively. The final products were dubbed MT for metal doped titania (M = V, Fe or Ni). The dried samples were sintered in a box furnace at different temperatures ranging from 450 to 800 °C for 2 h in an air atmosphere. The sintered samples were dubbed MT-calcination temperature. For example, samples calcined at 600 °C were dubbed VT600, FT600 and NT600. XRF analysis of the dried powder indicated that approximately 5.4, 5.8 and 6.1 percent of V_2O_5, Fe_2O_3 and NiO, respectively; were incorporated into TiO_2. During the preparation of pure TiO_2 powder (TT00), 10 mL of $TiOCl_2$ was added into 60 mL of DI water and stirred for 1 h followed by the addition of ammonium hydroxide to obtain a solid gel. The gel was peptized in 30 mL of 0.02 M nitric acid and stirred vigorously at room temperature for 2 h to obtain a TiO_2 sol. The pH of the sol was adjusted to 6 and the obtained slurry was aged at 80 °C for 4 h under constant stirring. The TiO_2 product was collected by filtration and dried at 100 °C for 6 h. The dried sample (TT00) was calcined at 450, 600 and 800 °C to yield TT450, TT600 and TT800 samples, respectively.

2.3. Photocatalytic test

Photocatalytic experiments of the M-TiO_2 samples were carried out to determine the practical reliability of the samples for decolorizing organic pollutants in the presence of natural sunlight. The photocatalytic experiments were carried out using the method described in our previous study [20]. In this particular test, glassware made from borosilicate glass (Pyrex) was used to minimize the absorption of UV light by the glass container [10,12]. 80 mL of a methylene blue (MB) solution (1×10^{-4} M) was placed into each Pyrex beaker followed by the addition of 0.8 g/L of the photocatalyst. Prior to exposure to sunlight, the suspensions were magnetically stirred in darkness for 1 h to establish adsorption-desorption equilibrium. The glass reactors were then exposed to sunlight (11.00 AM–3.00 PM). The experiments were carried out at Hanyang University, Ansan, Republic of Korea (37°17′49″N, 126°50′12″E) between 16th and 27th of September 2014 and the surrounding temperature was 24 °C. The suspensions were magnetically stirred while regularly withdrawing samples and then centrifuged (Heraeus Pico 17 centrifuge-Thermo Scientific, Germany) for UV analysis. The photocatalytic decolorization of MB was expressed as a function of the relative concentration of the MB solution (C/C_o) at a characteristic absorption of MB at 660 nm with reaction time; where C_o is the initial concentration and C is the concentration of MB solution absorption of MB at 660 nm at a time, t. A linear relationship between the logarithm of relative concentration of MB (Ln C_o/C) with the irradiation time (Ln $C_o/C = kt$) was used to estimate the decolorization rate constant (k) of the photocatalysts.

Reusability studies of the VT600, FT600 and NT600 photocatalysts was studied through carrying photocatalytic experiments in three consecutive runs. The samples were irradiated in the sunlight for 270 min and in every run the photocatalysts were recovered and reused to decolorize fresh MB solution. Moreover, the photocatalytic efficiencies of the tested samples was estimated from the equation; $(C_0 - C/C_0) \times 100\%$. In order to evaluate the generation of hydroxyl radicals (·OH) during photocatalysis another experiments was carried out. Briefly, 80 mL of 0.20 g/L terephthalic acid (TA) was prepared and 0.8 g/L of the photocatalyst was added to this and then stirred in the darkness for 1 h. This was subsequently irradiated in a natural sunlight environment under constant stirring. During this experiment 5 mL of the suspension was withdrawn regularly (every 30 min), centrifuged and the supernatant was scanned using Nanolog Spectrofluorometer (HORIBA) with an excitation at 315 nm from 350 nm to 600 nm.

2.4. Characterization

Bulk elemental analysis of the samples was carried out by an X-ray fluorescence spectrometer (XRF; XRF-1700, Shimadzu Co., Japan with a detection limit of 10 ppm and depth resolution of up to 10 μm). ZAF corrections (atomic number, Z) were used to determine the molar ratios of the elements present in the photocatalysts. An X-ray diffractometer (XRD-6000, Shimadzu) was used to study the crystalline properties of the photocatalysts using Cu Kα radiation (λ = 1.5406 Å). The accelerating voltage and applied current were 40 kV and 100 mA, respectively. The crystallite size of the powders was obtained by the Scherer equation [30]. The diffuse reflectance spectra (DRS) of the samples were recorded by a UV–vis spectrophometer (Shimadzu, UV-2600) between 200 and 900 nm using $BaSO_4$ as a reference. The photoelectron spectra of the samples were recorded by an X-ray photoelectron spectrometer (XPS; UVS-20-A, SPECS, Germany) using Al Kα X-ray source. A RENISHAW (RM 1000) Raman microscope was used to record Raman spectra of the samples using an He-Ne laser beam with wavelength of 632.8 nm.

The Brunauer–Emmett–Teller (BET) surface area and the porosity measurements of the calcined samples were studied by a N_2 adsorption-desorption instrument (Micrometrics ASAP 2020). All of the samples were degassed at 200 °C for 2 h prior to actual measurements. The pore size distribution (PSD) and specific desorption pore volumes were obtained using the Barrett-Joyner-Halenda (BJH) method, and desorption branches were used to determine the PSD. Field emission scanning electron microscopy (FE-SEM, Hitachi S-4800 Japan) with an accelerating voltage of 15.0 kV was used to study the morphology of the samples. The FE-SEM was coupled with energy dispersive spectroscopy (EDAX) to assess the purity and elemental composition of the samples that were synthesized in the present study. High-resolution transmission electron microscopy (HRTEM, Jeol JEM 2100F-Korea) was employed to study the distribution of particles in the photocatalysts. A UV–vis spectrometer (Optizen 2021 UV, Korea) was used to record the absorption spectra from 200 to 800 nm.

3. Results

3.1. Crystal structure

The phase structure and crystallite size of the samples were studied by powder XRD analysis. The XRD patterns for the as-synthesized samples and samples calcined at 450, 600 and 800 °C are presented in Figs. S1 and 1A–C, respectively. Fig. S1 shows that all of the as-synthesized samples were amorphous with the exception of the V-TiO_2 sample which showed the presence of anatase

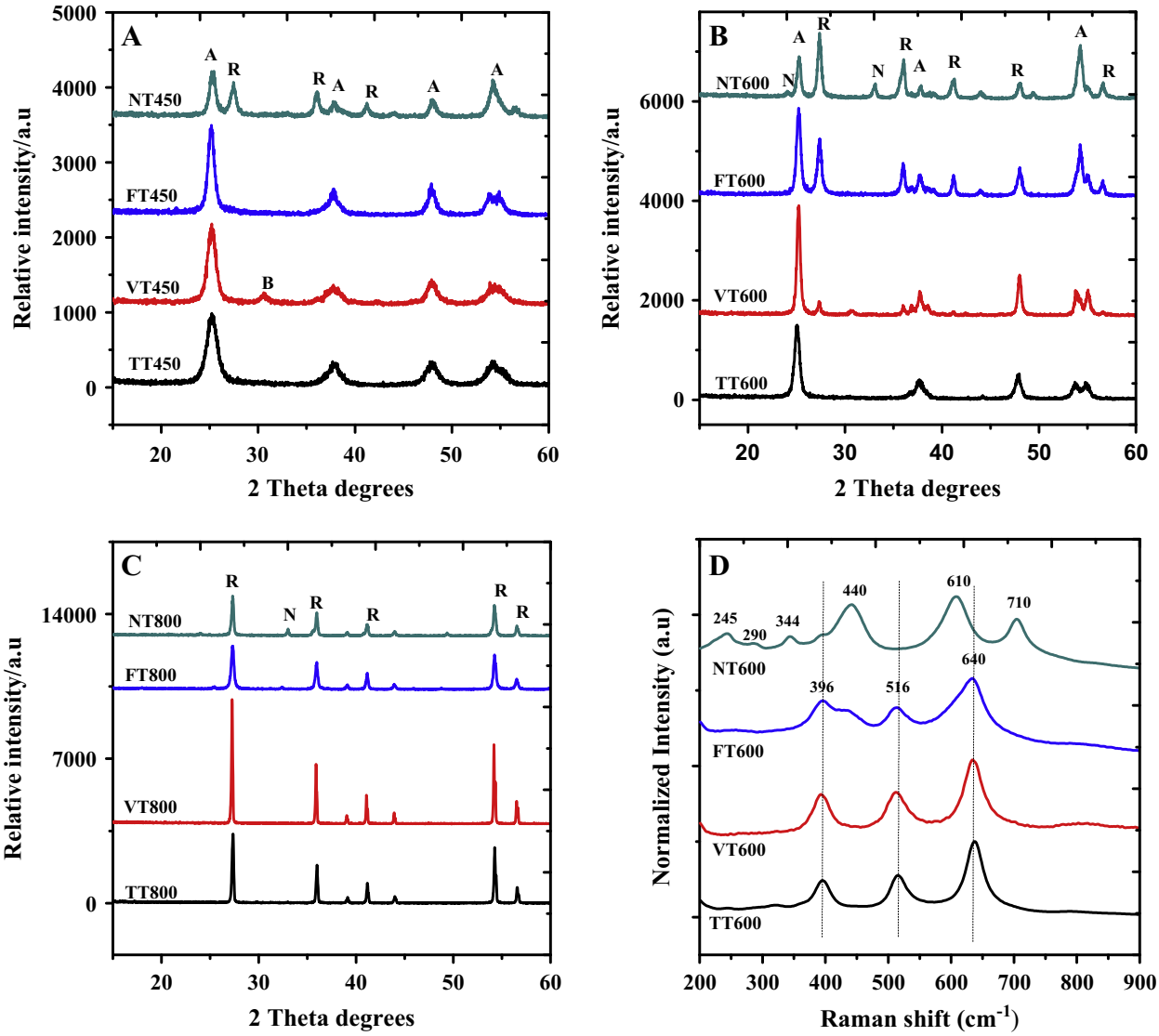


Fig. 1. XRD patterns of pure titania, Fe, Ni and V doped titania calcined at 450 °C (A) 600 °C (B) and 800 °C (C). The anatase phase (A), rutile (R), brookite (B) and $NiTiO_3$ (N) are indicated in the diffractograms. (D) Raman spectra of the samples calcined at 600 °C as representative samples.

and brookite TiO_2 crystals. Fig. 1A–C reveals that the calcined samples displayed different diffractograms indicating that the crystal structure of the samples were dependent upon the calcination temperature and the type of the dopant. Calcination of the samples at 450 °C led to the formation of various TiO_2 crystals. The TT450, VT450, FT450 and NT450 samples showed the presence of anatase TiO_2 crystals at ~25°, 38°, 48° and 56° [8,20,31]. In addition to the anatase peaks, a peak formed at ~31° in the VT450 sample signifying the existence of the brookite phase in the sample. On the other hand, the NT450 sample showed the presence of a mixture of both anatase and rutile TiO_2 crystals. Notable rutile peaks appear at ~27°, 36°, 47° and 54° [8,18]. This demonstrates that the presence of Ni^{2+} ions in the Ni-TiO_2 sample accelerates the formation of rutile at low calcination temperatures. Sintering of the samples at 600 °C leads to the anatase to rutile phase transformations (ART). Thus, all of the doped titania samples calcined at 600 °C possessed a mixture of anatase and rutile TiO_2 crystals. Additionally, the NT600 sample showed the occurrence of two peaks at 24.1° and 33.1°, which are assignable to $NiTO_3$ [32,33]. All of the samples sintered at 800 °C demonstrated a complete ART hence, only peaks for the rutile phase can be observed. Increasing the calcination temperatures increases the intensities of XRD peaks portraying that the grain size of the photocatalysts is also increased. Table 1 shows the crystallite size of the samples calcined at 450, 600 and 800 °C as were calculated by the Scherer' equation. The grain size of pure TiO_2 sample sintered at 450 °C was ~10 nm, this increased to 13 nm upon calcination at 600 °C. The grain size of the doped

Table 1
Crystallite size of the photocatalysts synthesized and calcined at different temperatures.

Calcination temperature (°C)	Titania phase	Sample name/crystallite size (nm)			
		TT	VT	FT	NT
450	Brookite	–	16.8	–	–
	Anatase	9.6	9.0	10.9	12.0
	Rutile	–	–	–	17.4
600	Brookite	–	21.8	–	–
	Anatase	13.0	20	15.8	17.5
	Rutile	–	27	16.8	17.4
800	Brookite	–	–	–	–
	Anatase	–	–	26.5	–
	Rutile	41.0	58.8	25.5	34.0

TiO_2 in the samples calcined at 450–600 °C was between 9 and 22 nm. The grain size of the TT800 sample was 41 nm whereas those of the doped TiO_2 samples were between 25 and 59 nm. Generally, the crystallite size of these samples increased as the calcination temperature was increased.

3.2. Raman spectroscopy

The formation of different phases in the photocatalysts was further investigated by Raman spectroscopy. Fig. 1D shows the Raman spectra of pure TiO_2 and doped TiO_2 samples sintered at 600 °C. The TT600 and VT600 samples show prominent Raman lines at 396, 516 and 639 cm^{-1} which are assignable to the B_1, B_{1g} and A_{1g} vibration modes of anatase TiO_2 crystal, respectively [28,34]. The XRD pattern of the VT600 sample showed the presence of a mixture of anatase, brookite and rutile; however, the vibration peaks attributable to rutile and brookite were not observed which might be due to their low intensities. The TF600 and NT600 samples showed the presence of vibration modes for both anatase and rutile TiO_2. In addition to the Raman lines of anatase at 396, 516 and 639 cm^{-1}, the vibrations at 245–290, 394, 440, 610 and 710 cm^{-1} indicate the presence of the rutile phase in these materials [33].

3.3. Diffuse reflectance spectroscopy

The interaction between Ti, V, Fe and Ni in the photocatalysts was investigated by UV–vis DRS. The reflectance spectra were transformed to Kubelka-Munk coordinates (KM, α) and then Tauc's plots were constructed from (KM. hυ) ^{½} against hυ. The indirect band gap energies were estimated by extrapolating the linear portion of the Tauc's plots onto the hυ axis [5,21,26]. The UV–vis DRS spectra and their corresponding Tauc's plots of representative samples calcined at 600 °C are presented in Fig. 2. Fig. 2A reveals that pure titania sample calcined at 600 °C demonstrated a strong absorption below 415 nm, which is a result of ligand-to-metal charge transfer between the O^{2-} ligand and the Ti^{4+} ion [31,35]. However, the doped TiO_2 samples show significant absorption edges at $\lambda \geqslant 450$ nm which covers the visible region indicating the formation of visible light active (VLA) photocatalysts [17,26].

The optical properties of these samples demonstrate that the shifting of the absorption properties to low energies is attributable to the dopants that are incorporated in the photocatalysts [1,3,22,29,32,36–38]. The spectrum for the NT600 sample shows a broad absorption edges at 418 nm due to the optical band gap that is attributed to the O^{2-} ligand and the Ti^{4+} charge transfer interaction. The two absorption band of this spectrum at 450 and 508 nm are due to crystal field splitting caused by the $Ni^{2+} \rightarrow Ti^{4+}$ charge transfer interaction [32]. The band gap energy (E_g) registered by the TT600 sample was ~3.16 eV which is the typical band gap energy for the anatase structure (Fig. 2B). On the other hand, the band gap energies of the doped TiO_2 samples w (~2.1–2.8 eV) were considerably lower than that of the TT600 sample (Table 2). These experimental results signify that the samples can possibly be activated by visible light; therefore, they can be used as heterogeneous photocatalysts in the presence of natural solar irradiation [1,21,22,29,36].

3.4. X-ray photoelectron spectroscopy

Fig. 3 displays the high-resolution XPS spectra of the doped titania samples calcined at 600 °C to determine their chemical states. The photoelectron peaks attributable to the chemical states of Ti $2p_{3/2}$ and Ti $2p_{½}$ appear at 458.1 eV and 463.6 eV, respectively, implying the existence of Ti^{4+} species. The existence of the bulk oxygen of metallic oxides in the samples is substantiated by the appearance of the O 1s photoelectron peak at 529.7 eV (Fig. S2). Fig. 3B verifies the incorporation of V^{5+} species into TiO_2 due to the formation of the V $2p_{3/2}$ peak at 516.4 eV. It was formerly [25,39] reported that the binding energies of V^{5+} $2p_{3/2}$ (516.4–517.4 eV) and V^{4+} $2p_{3/2}$ (515.4–515.7 eV) are very close; thus, it is possible that the V-TiO_2 samples also contain V^{4+} species. The high resolution XPS spectrum in Fig. 3C shows the formation of a broad peak for Fe $2p_{3/2}$ at 710.5 eV indicating the presence of Fe^{3+} species in the Fe-TiO_2 photocatalysts [3]. The NT600 samples (Fig. 3D) displayed peaks assignable to Ni $2p_{3/2}$ and Ni $2p_{½}$ at 855.4 eV and 873.0 eV, respectively indicating the presence of Ni^{2+} ions in the Ni-TiO_2 sample [20,32].

3.5. Nitrogen gas physisorption studies

The textural properties of the samples were investigated by nitrogen gas adsorption-desorption method at 77 K. Fig. 4A presents the N_2 adsorption-desorption isotherms of TT600, VT600,

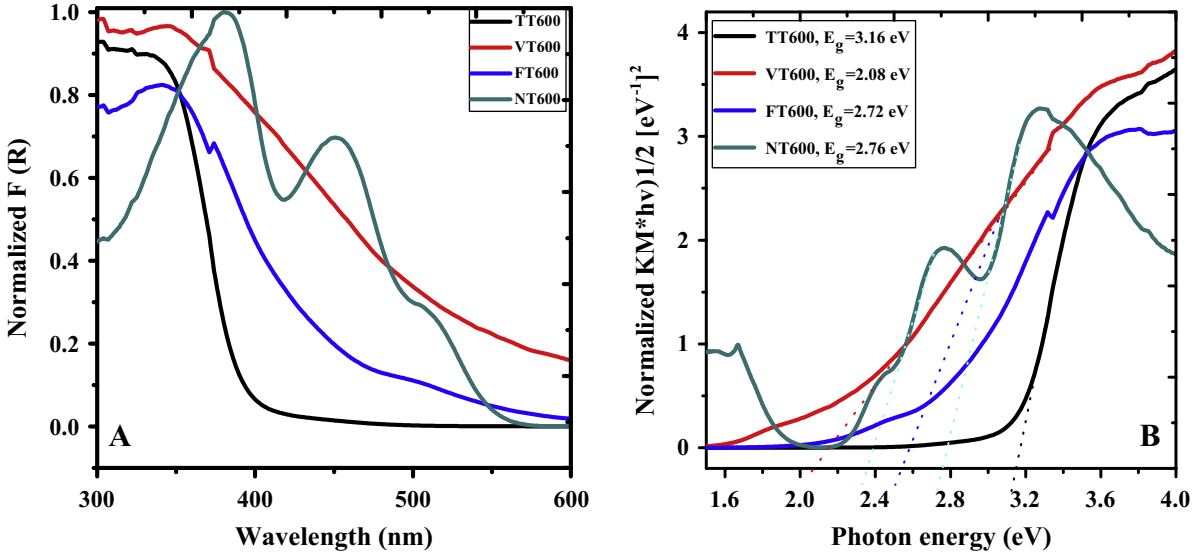


Fig. 2. DRS spectra (A) and their respective band gaps (B) of pure titania V, Fe and Ni doped titania calcined at 600 °C.

Table 2
Physicochemical properties of the photocatalysts synthesized and calcined at 600 °C.

Sample name	E_g (eV)	Surface area (m^2/g)	Pore volume (cm^3/g)	Pore diameter (nm)	Rate constant (min^{-1})	R^2
TT600	3.16	88	0.15	4.8	0.0010	0.9722
VT600	2.08	27	0.07	8.5	0.0125	0.9910
FT600	2.72	33	0.08	13.4	0.0028	0.9965
NT600	2.76	38	0.18	19.0	0.0078	0.9585

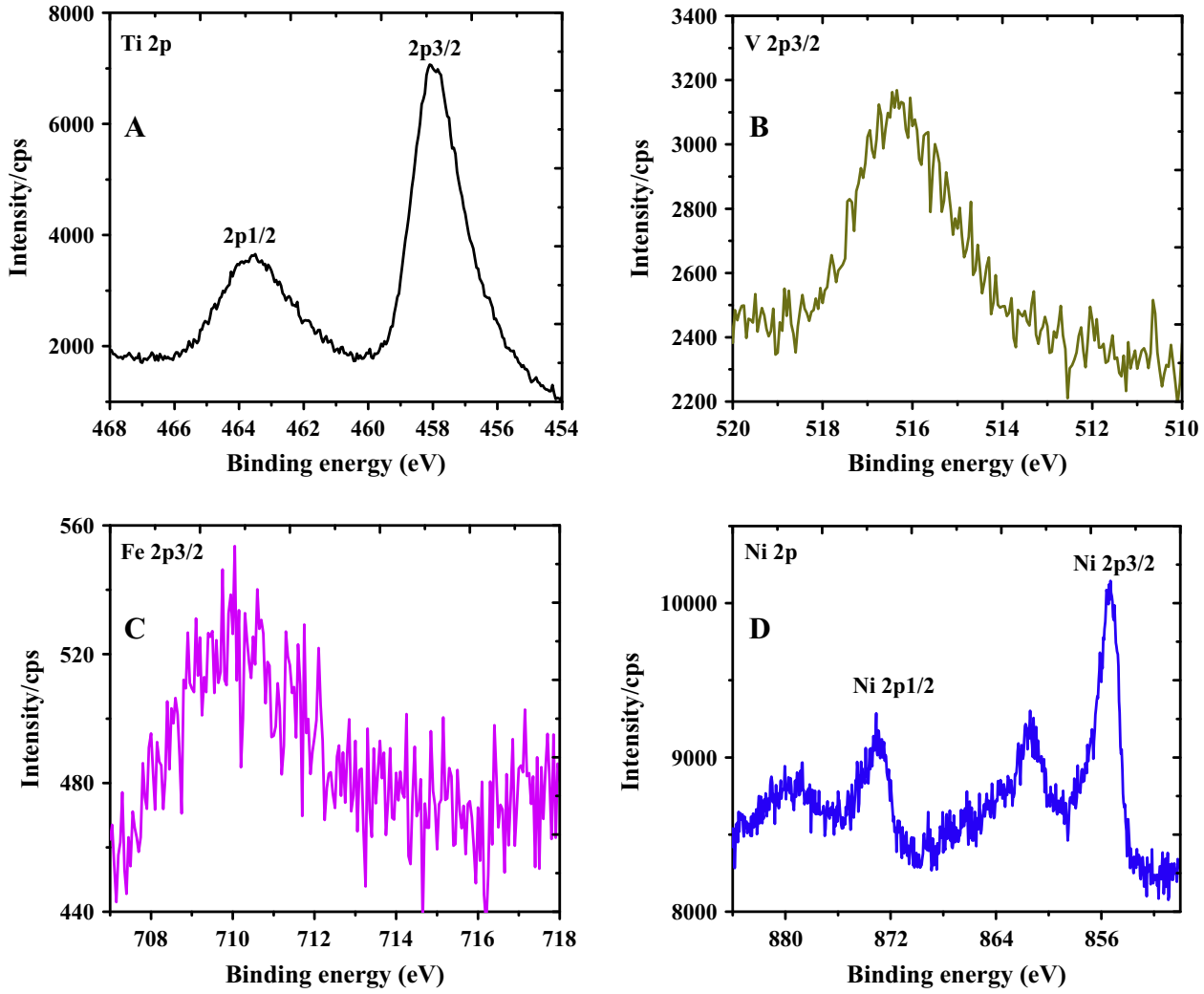


Fig. 3. High resolution XPS spectra of the doped samples showing the presence of Ti, V, Fe and Ni in the samples obtained and calcined at 600 °C.

FT600 and NT600 as the representative samples. Table 2 shows the specific surface areas and textural properties of the samples calcined at 600 °C as representative samples. The specific surface areas of pure TiO_2 and metal doped TiO_2 calcined at 600 °C were between 27 and 88 m^2/g. The pore diameters of the doped TiO_2 samples were larger than that of pure TiO_2. Fig. 4A indicates that all samples exhibited Type IV isotherm curves signifying the presence of mesoporous structures associated with capillary condensation of the adsorbent [9,10,12,20,40–42]. The nitrogen gas uptake of the TT600 and VT600 samples are centered at relative pressures of $0.5 < P/Po < 0.85$ demonstrating the absence of macropores. However, the FT600 and NT600 samples show isotherm with a sharp uptake near $P/P_0 = 1$ indicating the presence of some macropores. It is also noticeable that theTT600 and VT600 samples exhibited hysteresis loops that are very similar to type H2 according to the IUPAC classification systems portraying the presence of aggregates with uniform channel-like pores [9,40–44].

The NT600 sample exhibited a type H3 hysteresis loop indicating the presence of aggregates of plate-like particles or the assemblage of slit-shaped pores with unlimited adsorption of the adsorbent at high P/Po with a characteristic step-down in the desorption branch that is associated with hysteresis closure at low relative pressures ($P/Po < 0.1$). A type H4 hysteresis loop was displayed by the FT600 sample implying the existence of narrow, slit-like pores [9,12,42]. Fig. 4B display the pore size distribution (PSD) of both pure TiO_2 and doped TiO_2 samples calcined at 600 °C as representative samples. It can be seen that the TT600 and VT600 samples demonstrated a narrow PSD between 3 and

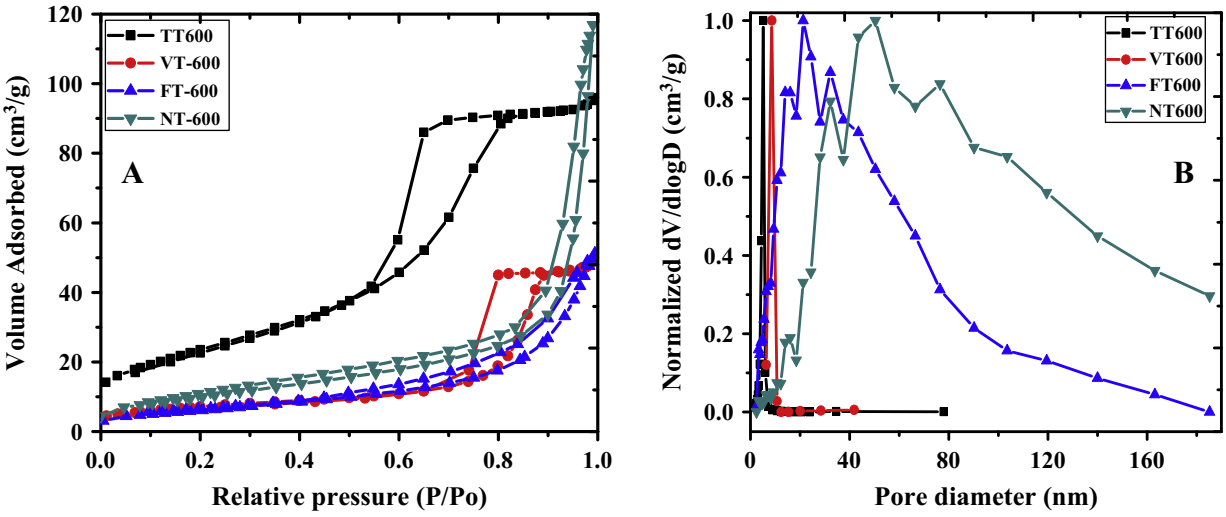


Fig. 4. N_2 adsorption-desorption isotherms (A) and pore size distribution (B) of pure titania, V, Fe and Ni doped titania calcined at 600 °C.

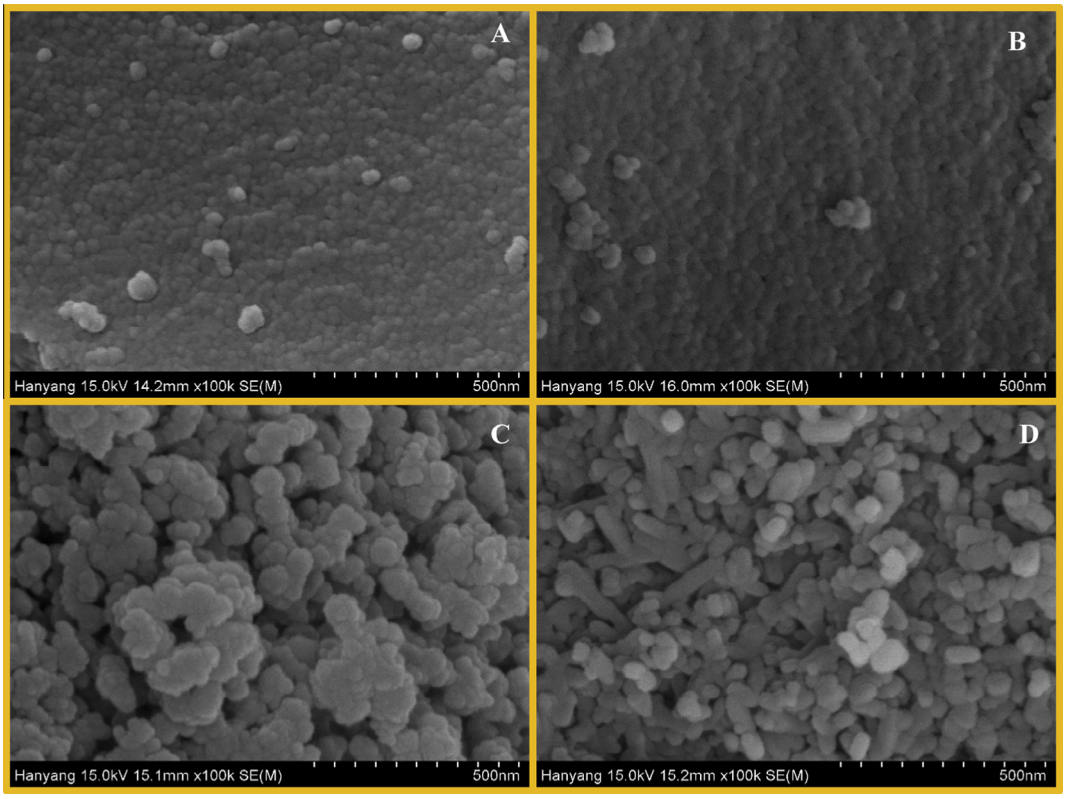


Fig. 5. SEM images of TT600, VT600, FT600 and NT600 as representative sample of pure and doped TiO_2 photocatalysts.

15 nm. Nonetheless, the broad PSD of the FT600 and NT600 samples from 10 to 80 nm exemplifies the presence of mesopores and perhaps macropores [9,40].

3.6. Morphology of the samples

The morphologies of the photocatalysts obtained through two-step sol-gel process were studied by SEM, STEM and TEM analyses. SEM was coupled with EDAX to study the elemental composition of the photocatalysts. The EDAX results of the doped titania photocatalysts calcined at 600 °C are compiled in Fig. S3. It can be seen that the photocatalysts showed the presence of Ti, V, Ni, Fe and O; these results are congruent with the XRF and XPS analyses. Fig. 5A–D shows SEM images of the selected representative samples calcined at 600 °C. TT600 and VT600 samples possessed spherical primary particles with a diameter less than 30 nm; the latter exhibits more regular primary particles (Fig. 5A and B). Fig. 5C and D reveals that the FT600 and NT600 samples exhibited highly porous structure and primary particles of different size and shape. The FT600 sample shows the existence of clusters of spherical particles. The TEM image of the FT600 sample in Fig. 6A demonstrates that the diameters of these particles are less than 30 nm. TEM image (Fig. 6C) and STEM image (Fig. S3D) show that the NT600 sample exhibited both rod-like and spherical particles. Fig. S4 illustrates

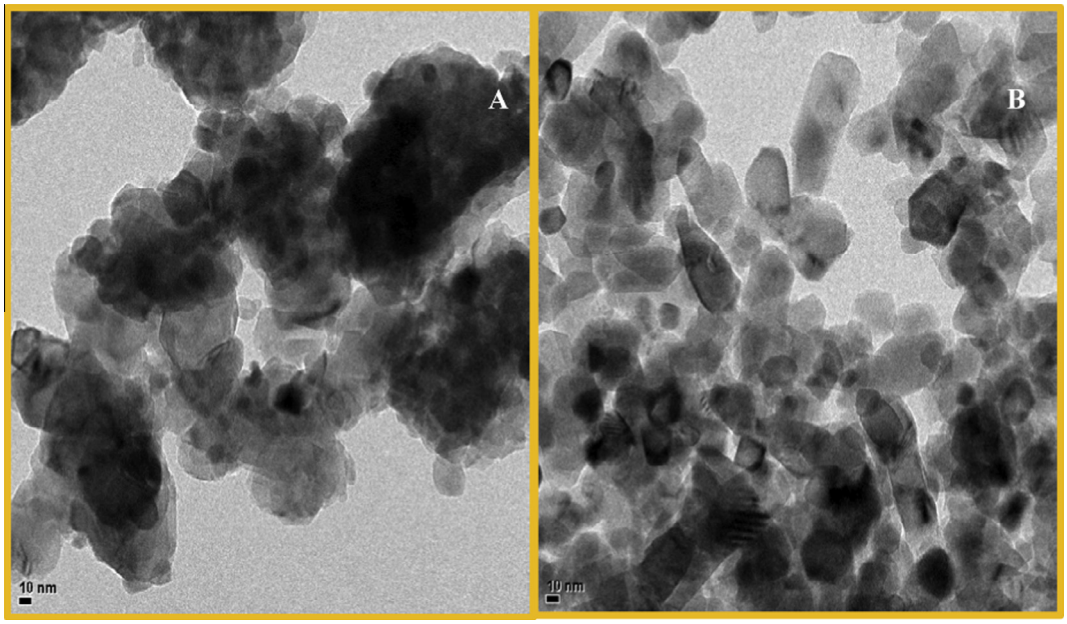


Fig. 6. TEM micrographs of the FT600 and NT600 exemplifying the formation of grains with different shapes and dispersion.

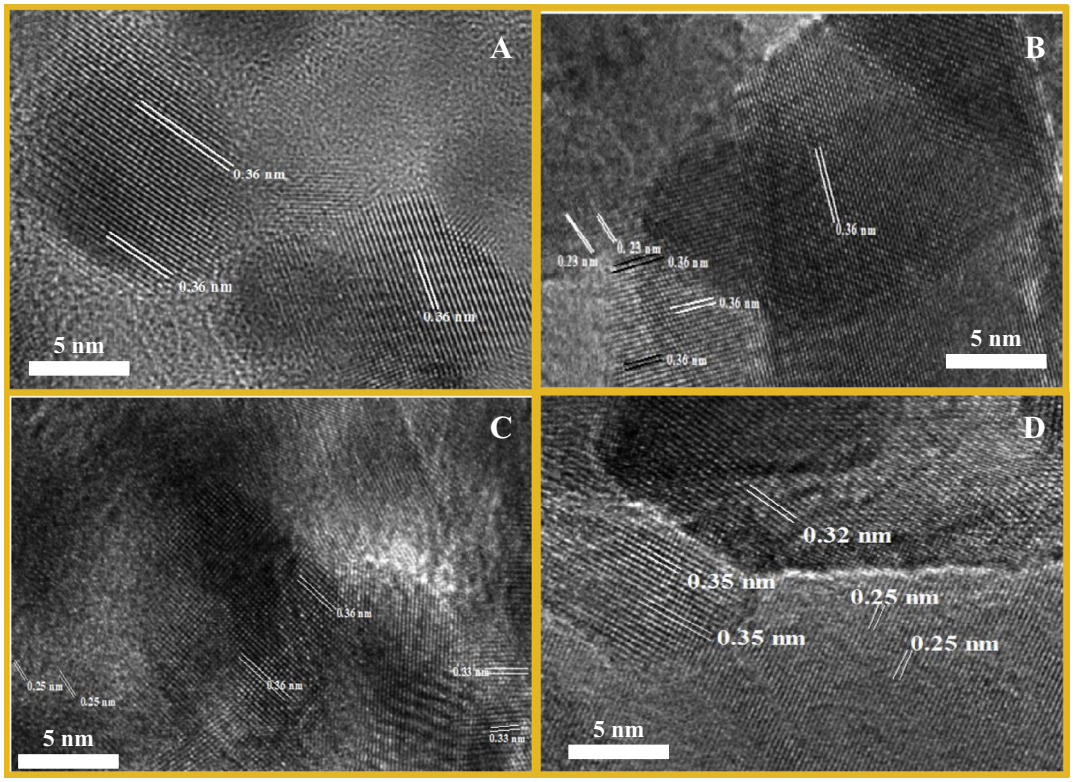


Fig. 7. HRTEM of TT600, VT600, FT600 and NT600 samples illustrating the presence of various lattice fringes of crystals.

that further calcination of the samples at 800 °C increased their particle size (FT800 and NT800 are presented as representative samples).

Fig. 7 shows the high-resolution TEM image of pure and doped TiO_2 samples fired at 600 °C. Fig. 7A shows clear lattice fringes of anatase TiO_2 crystals (0.36 nm). On the other hand, HRTEM micrographs of the doped samples showed the presence of lattice fringes for V_2O_5 (0.23 nm), Fe_2O_3 (0.25 nm) and $NiTiO_3$ (0.25 nm) domains (Fig. 7C and D) in the photocatalysts calcined at 600 °C. Other prominent features in these HRTEM images are the lattice fringes of both anatase (0.36 nm) and rutile (0.32 nm) that can be recognized in the FT600 and NT600 samples. This observation is in good agreement with the XRD results (Fig. 1B) which indicated that a mixture of anatase and rutile TiO_2 crystals were obtained in the samples calcined at 600 °C. However, rutile TiO_2 crystals were not identified in the VT600 samples which might be due to the fact

that rutile is only presents in a small amount. The occurrence of well-defined inter-faces between these crystals can also be noticed. This interaction might be beneficial to in the formation of samples with improved photochemical performances [13,18,32].

3.7. Photocatalytic properties

The photochemical performance of the samples synthesized in the present study was tested in the degradation of a methylene blue solution in the presence of natural sunlight. The samples calcined at 600 °C were used as representative samples to investigate the photochemical efficiency of the obtained photocatalysts due to their unique properties such as well-developed crystal structure, porous structures, well-defined inter-faces between crystals and the existence of less aggregated particles. Fig. 8 presents the photoactivity of the representative samples of the photocatalysts obtained and calcined at 600 °C in the presence of solar irradiation. It can be noticed that the degradation by undoped TiO_2 was less than 25% whilst the doped TiO_2 displayed higher degradation efficiencies. The VT600 sample exhibited the highest activity as up to ~97% of the MB was decolorized in the presence of this particular photocatalyst. Fig. 8B shows the linear relationship between the logarithms of the relative concentration of the MB solution (Ln C_o/C) against the reaction time of the TiO_2 and M-TiO_2 samples calcined at 600 °C. The slope of this plot correspond to the rate constant for each photocatalysts. By comparing the rate constant of these sample, it was deduced that the activities of the samples increased in the order; TT600 < FT600 < NT600 < VT600. This signifies that doping TiO_2 with various transition metals leads to the formation of photocatalysts with improved activities [20,22,26,33]. The experimental results from reusability studies of the VT600, FT600 and NT600 photocatalysts are shown in Fig. 9. It is noteworthy that the samples showed a little deterioration (~2–5%) after samples were recycled for three consecutive runs.

The photochemical properties of metal oxide photocatalysts depend on the generation of photogenerated charge carriers, the separation of electron-hole pairs and efficiency of charge carrier transfer [20,26,31,41,45,46]. It was previously reported [47–50] that hydroxyl radicals are highly oxidative species that are

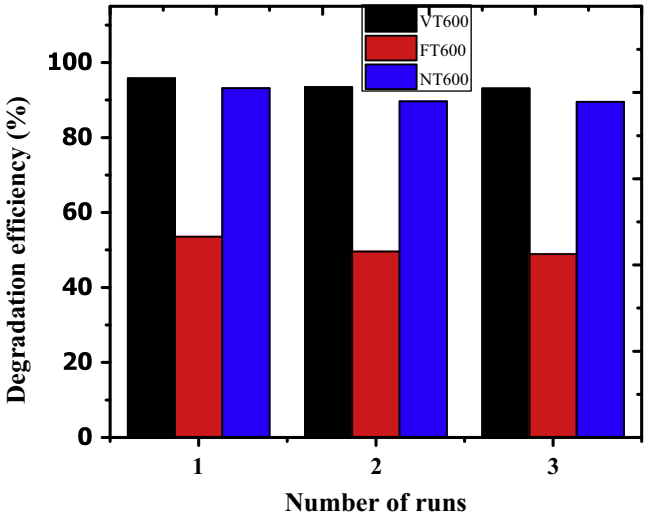


Fig. 9. Investigation of the reusability of the VT600, FT600 and NT600 photocatalysts as representative samples.

considered to be the main species responsible for the photodegradation of the organic contaminants either adsorbed on the surface of the photocatalyst or in the bulk solution. Hence, the generation of hydroxyl radicals (·OH) during the photocatalytic process was monitored through irradiating a solution containing terephthalic acid and VT600 photocatalysts as a representative sample. Fig. 10 demonstrates that the fluorescence intensity of the solution at 436 nm increased as the irradiation time increased. This signifies that the highly fluorescent 2-hydroxyterephthalic acid compound was formed during solar irradiation due to the generation of ·OH species.

4. Discussion

The modification of TiO_2 with transition metals yields VLA photocatalysts thus, the photocatalytic activity can presumably be improved through this strategy [17,24,34]. The present study

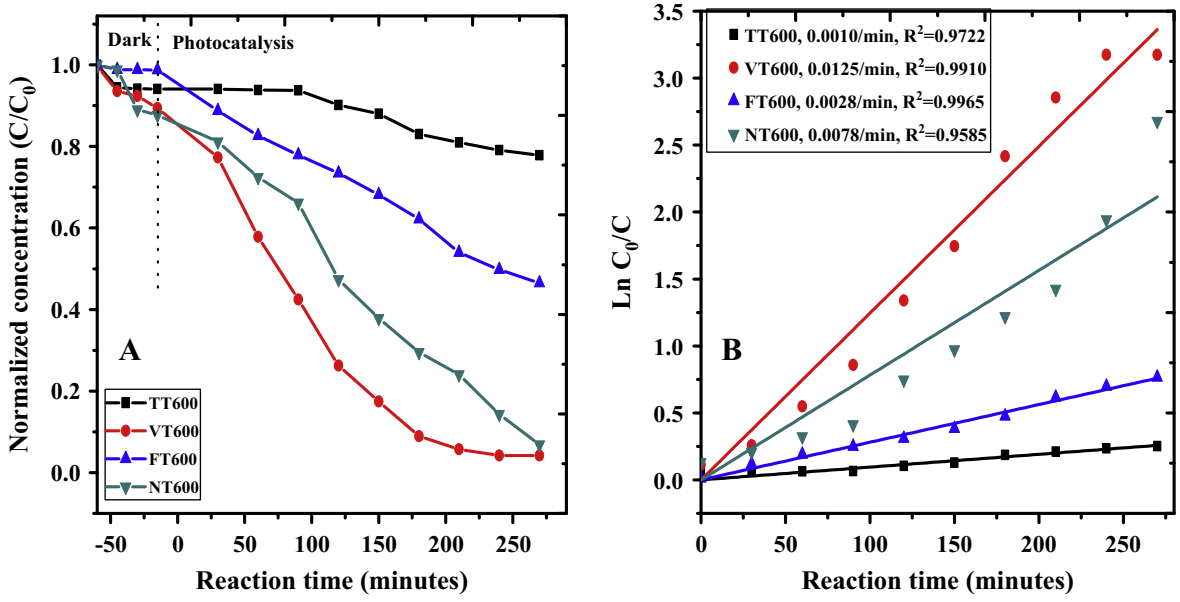


Fig. 8. Photocatalytic properties of pure TiO_2, V, Fe and Ni doped titania calcined at 600 °C in the presence of natural solar irradiation (A) a linear relationship between the logarithms of relative concentration of MB solution (Ln Co/C) against the reaction time of the titania and doped titania for samples calcined at 600 °C (B).

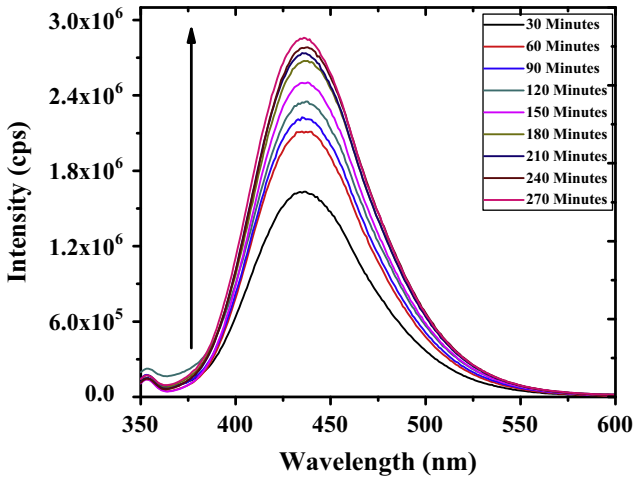


Fig. 10. Photofluorimetry spectral changes with time in the Terephthalic acid solution during natural sunlight irradiation in the presence of the VT600 as a representative photocatalyst.

proposed a convenient sol-gel method to obtain V, Fe and Ni doped TiO_2 samples with different physicochemical properties. Structural characterization depicted that highly porous materials with well-developed crystalline structure (after sintering) were obtained. SEM results demonstrated that doping and subsequent calcination of the as-synthesized samples alters both the shape and particle size. Initially, the as-synthesized samples (not presented) possessed small and spherical primary aggregates. Sintering these samples facilitated particle growth and consequent formation of mesostructure with less aggregated particles. It was also observed that the shape of the particles was also influenced by calcination temperatures. The NT600 sample showed that rod-like particles can be attained upon sintering.

XRD results (Fig. 1B) revealed that sintering of the doped samples at temperatures $\leqslant$600 °C led to the formation of a mixture of anatase and rutile TiO_2 nanocrystals (Fig. 1B). Ahmed et al. [51] reported on the synthesis of Fe_2O_3-TiO_2 nanoparticles by a sol–gel method and evaluated their photocatalytic properties. It was found that the presence of Fe_2O_3 in the samples accelerates the ART which harnessed the photocatalytic performance of the samples indeed. Ganesh et al. [33] investigated the influence of Ni^{2+} on the mesostructure of TiO_2. They found that the presence of different amounts of Ni^{2+} ions could either stabilize the anatase phase or promote the ART. The ionic radii-valance concept has been used to explain the mechanism by which cationic dopants promote the ART. It has been suggested that cationic dopants with small radii and low valence can substitute and occupy the lattice sites of Ti^{4+} ions. This process increases the number of oxygen vacancies and accelerate the ART [15]. The experimental results of the present study concur with former reports on the context that the presence of amount of V^{5+}, Fe^{3+} and Ni^{2+} species in the mesostructure of TiO_2 promotes the ART. Thus, the crystal structure of the samples obtained in the present study was largely dependent on the nature of the dopant and the calcination temperatures.

Based on previous reports [22,29], dopant oxides can be incorporated on the TiO_2 surface by anchoring onto surface available hydroxyl groups. Sintering facilitates the stabilization of the obtained photocatalyst. Further studies [15,34] have pointed out that the presence of metal dopants present in TiO_2 systems can act as both electron traps and hole traps. They can also engage in charge release and migration to the interface of a solid-liquid reaction system. Generally, the presence of metal dopants generates a new energy level in the band gap of TiO_2. Their presence reduces the energy required to excite electron from the valance band to the conduction band; therefore, it is possible to evaluate the photocatalytic activities of the samples in the presence of sunlight [22]. Optical analysis of the samples obtained in the present study depicted that the incorporation of V^{5+}, Fe^{3+} and Ni^{2+} into TiO_2 extended the optical absorption of the photocatalysts to the visible region (E_g = ~2.2–2.5 eV).

The photocatalytic results of the present study (Fig. 8) indicated that the activities of the obtained samples were in the order TT600 < TF600 < NT600 < VT600. This demonstrates that the activity of Ni-TiO_2 was higher than that of the Fe-TiO_2 sample (Fig. 10). It is thought that the unique photochemical performance of the NT600 sample was due to the homogeneous dispersion of NiO in TiO_2 to form $NiTiO_3$ species [32,33]. Qu et al. [32] found that porous $NiTiO_3$ nanorods exhibit good photocatalytic performance in the presence of visible light. Therefore, it can be assumed that the photochemical performance of the obtained samples was influenced by the morphology, porous structure, a mixture of TiO_2 crystals, homogeneous dispersion and the improved optical properties [17,19,33,52]. However, the possibility to use a convenient sol-gel preparation technique to introduce transition metal into TiO_2 is exceedingly interesting and it will help to promote large-scale production of heterogeneous photocatalysts.

5. Conclusions

In the present report the photochemical performances of V, Fe and Ni doped TiO_2 photocatalysts were systematically compared. The photocatalysts were synthesized by a controllable, cost-effective and versatile sol-gel approach using titanium oxychloride as a titania source and in the absence of surfactants. The experimental results showed that samples with different physicochemical properties can be obtained depending on the type of dopant and the calcination temperature. Structural characterizations substantiated the incorporation of V^{5+}, Fe^{3+} and Ni^{2+} into titania to yield highly photoactive materials. XRD analysis showed that the presence of the metal dopants accelerated the anatase to rutile phase transformation at low calcination temperatures. SEM and TEM analyses showed that samples with less aggregated particles and improved optical properties were produced due to the presence of V_2O_5, Fe_2O_3 and NiO. Thus, samples exhibited superior properties (phase structure, crystallinity, crystallite size, morphology and porous structure) that are desirable for heterogeneous photocatalysis in the presence of natural sunlight. The photocatalytic test of the calcined samples revealed that the activities of M-TiO_2 were higher that of pure titania and the VT600 sample possessed the highest activity of all of the samples due to its superior properties. We anticipate that this systematic investigation of VLA photocatalysts will enhance the large-scale industrial production of cost-effective heterogeneous photocatalysts with desirable properties for the degradation of organic pollutants that are produced by textile industries.

Acknowledgement

This work was supported by the research fund of Hanyang University (HY-2015-P).

Appendix A. Supplementary material

Supplementary data associated with this article can be found, in the online version, at http://dx.doi.org/10.1016/j.jcis.2016.04.024.

References

[1] J.I. Peña-Flores, A.F. Palomec-Garfias, C. Márquez-Beltrán, E. Sánchez-Mora, E. Gómez-Barojas, F. Pérez-Rodríguez, Fe effect on the optical properties of TiO_2:Fe_2O_3 nanostructured composites supported on SiO_2 microsphere assemblies, Nanoscale Res. Lett. 9 (2014) 499.

[2] Z. Li, D. Ding, Q. Liu, C. Ning, X. Wang, Ni-doped TiO_2 nanotubes for wide-range hydrogen sensing, Nanoscale Res. Lett. 9 (2014) 118.

[3] J. Yu, Q. Xiang, M. Zhou, Preparation, characterization and visible-light-driven photocatalytic activity of Fe-doped titania nanorods and first-principles study for electronic structures, Appl. Catal. B 90 (2009) 595–602.

[4] A. Fujishima, K. Honda, Electrochemical photolysis of water at a semiconductor electrode, Nature 238 (1972) 37–38.

[5] A. Fujishima, X. Zhang, D.A. Tryk, TiO_2 photocatalysis and related surface phenomena, Surf. Sci. Rep. 63 (2008) 515–582.

[6] K. Nakata, A. Fujishima, TiO_2 photocatalysis: design and applications, J. Photochem. Photobiol., C 13 (2012) 169–189.

[7] E. Comini, C. Baratto, G. Faglia, M. Ferroni, A. Vomiero, G. Sberveglieri, Quasi-one dimensional metal oxide semiconductors: preparation, characterization and application as chemical sensors, Prog. Mater. Sci. 54 (2009) 1–67.

[8] G.L. Chiarello, E. Selli, L. Forni, Photocatalytic hydrogen production over flame spray pyrolysis-synthesised TiO_2 and Au/TiO_2, Appl. Catal. B 84 (2008) 332–339.

[9] G.N. Shao, Y. Kim, S.M. Imran, S.J. Jeon, P.B. Sarawade, A. Hilonga, J.-K. Kim, H.T. Kim, Enhancement of porosity of sodium silicate and titanium oxychloride based TiO_2–SiO_2 systems synthesized by sol–gel process and their photocatalytic activity, Microporous Mesoporous Mater. 179 (2013) 111–121.

[10] G.N. Shao, A. Hilonga, S.J. Jeon, J.E. Lee, G. Elineema, D.V. Quang, J.-K. Kim, H.T. Kim, Influence of titania content on the mesostructure of titania–silica composites and their photocatalytic activity, Powder Technol. 233 (2013) 123–130.

[11] A.A. Ismail, D.W. Bahnemann, Mesoporous titania photocatalysts: preparation, characterization and reaction mechanisms, J. Mater. Chem. 21 (2011) 11686–11707.

[12] G.N. Shao, G. Elineema, D.V. Quang, Y.N. Kim, Y.H. Shim, A. Hilonga, J.-K. Kim, H.T. Kim, Two step synthesis of a mesoporous titania–silica composite from titanium oxychloride and sodium silicate, Powder Technol. 217 (2012) 489–496.

[13] B.K. Mutuma, G.N. Shao, W.D. Kim, H.T. Kim, Sol–gel synthesis of mesoporous anatase–brookite and anatase–brookite–rutile TiO_2 nanoparticles and their photocatalytic properties, J. Colloid Interface Sci. 442 (2015) 1–7.

[14] H. Zhang, J.F. Banfield, Understanding polymorphic phase transformation behavior during growth of nanocrystalline aggregates: insights from TiO_2, J. Phys. Chem. B 104 (2000) 3481–3487.

[15] D.A. Hanaor, C.C. Sorrell, Review of the anatase to rutile phase transformation, J. Mater. Sci. 46 (2011) 855–874.

[16] L.-L. Tan, W.-J. Ong, S.-P. Chai, A.R. Mohamed, Visible-light-activated oxygen-rich TiO_2 as next generation photocatalyst: importance of annealing temperature on the photoactivity toward reduction of carbon dioxide, Chem. Eng. J. 283 (2016) 1254–1263.

[17] M. Pelaez, N.T. Nolan, S.C. Pillai, M.K. Seery, P. Falaras, A.G. Kontos, P.S. Dunlop, J.W. Hamilton, J.A. Byrne, K. O'Shea, A review on the visible light active titanium dioxide photocatalysts for environmental applications, Appl. Catal. B 125 (2012) 331–349.

[18] G.N. Shao, A. Hilonga, Y.N. Kim, J.-K. Kim, G. Elineema, D.V. Quang, S.J. Jeon, H. T. Kim, Peptization technique in the synthesis of titania–silica composites and their photocatalytic properties, Chem. Eng. J. 198–199 (2012) 122–129.

[19] T. Ohno, K. Tokieda, S. Higashida, M. Matsumura, Synergism between rutile and anatase TiO_2 particles in photocatalytic oxidation of naphthalene, Appl. Catal. A 244 (2003) 383–391.

[20] G.N. Shao, S.M. Imran, S.J. Jeon, S.J. Kang, S.M. Haider, H.T. Kim, Sol–gel synthesis of vanadium doped titania: effect of the synthetic routes and investigation of their photocatalytic properties in the presence of natural sunlight, Appl. Surf. Sci. 351 (2015) 1213–1223.

[21] R.-A. Doong, P.-Y. Chang, C.-H. Huang, Microstructural and photocatalytic properties of sol–gel-derived vanadium-doped mesoporous titanium dioxide nanoparticles, J. Non-Cryst. Solids 355 (2009) 2302–2308.

[22] A. Zaleska, Doped-TiO_2: a review, Recent Patents Eng. 2 (2008) 157–164.

[23] M. Meyer, L.C. Damonte, Study of Co and Fe-doped ZnO milled nanopowders, Powder Technol. 286 (2015) 371–377.

[24] D.M. Tobaldi, A. Sever Škapin, R.C. Pullar, M.P. Seabra, J.A. Labrincha, Titanium dioxide modified with transition metals and rare earth elements: phase composition, optical properties, and photocatalytic activity, Ceram. Int. 39 (2013) 2619–2629.

[25] X. Yang, F. Ma, K. Li, Y. Guo, J. Hu, W. Li, M. Huo, Y. Guo, Mixed phase titania nanocomposite codoped with metallic silver and vanadium oxide: new efficient photocatalyst for dye degradation, J. Hazard. Mater. 175 (2010) 429–438.

[26] M. Anpo, M. Takeuchi, The design and development of highly reactive titanium oxide photocatalysts operating under visible light irradiation, J. Catal. 216 (2003) 505–516.

[27] L. Yu, S. Yuan, L. Shi, Y. Zhao, J. Fang, Synthesis of Cu^{2+} doped mesoporous titania and investigation of its photocatalytic ability under visible light, Microporous Mesoporous Mater. 134 (2010) 108–114.

[28] J.I. Peña-Flores, A.F. Palomec-Garfias, C. Márquez-Beltrán, E. Sánchez-Mora, E. Gómez-Barojas, F. Pérez-Rodríguez, Fe effect on the optical properties of TiO_2:Fe_2O_3 nanostructured composites supported on SiO_2 microsphere assemblies, Nanoscale Res. Lett. 9 (2014) 1–7.

[29] M.A. Bañares, L.J. Alemany, M.C. Jiménez, M.A. Larrubia, F. Delgado, M. López Granados, A. Martínez-Arias, J.M. Blasco, J.L.G. Fierro, The role of vanadium oxide on the titania transformation under thermal treatments and surface vanadium states, J. Solid State Chem. 124 (1996) 69–76.

[30] S. Tanemura, L. Miao, P. Jin, K. Kaneko, A. Terai, N. Nabatova-Gabain, Optical properties of polycrystalline and epitaxial anatase and rutile TiO_2 thin films by rf magnetron sputtering, Appl. Surf. Sci. 212–213 (2003) 654–660.

[31] G.N. Shao, M. Engole, S.M. Imran, S.J. Jeon, H.T. Kim, Sol–gel synthesis of photoactive kaolinite-titania: effect of the preparation method and their photocatalytic properties, Appl. Surf. Sci. 331 (2015) 98–107.

[32] Y. Qu, W. Zhou, Z. Ren, S. Du, X. Meng, G. Tian, K. Pan, G. Wang, H. Fu, Facile preparation of porous $NiTiO_3$ nanorods with enhanced visible-light-driven photocatalytic performance, J. Mater. Chem. 22 (2012) 16471–16476.

[33] I. Ganesh, A. Gupta, P. Kumar, P. Sekhar, K. Radha, G. Padmanabham, G. Sundararajan, Preparation and characterization of Ni-doped TiO_2 materials for photocurrent and photocatalytic applications, Sci. World J. 2012 (2012).

[34] J. Zhou, Y. Zhang, X.S. Zhao, A.K. Ray, Photodegradation of benzoic acid over metal-doped TiO_2, Ind. Eng. Chem. Res. 45 (2006) 3503–3511.

[35] O.Y. Gutiérrez, G.A. Fuentes, C. Salcedo, T. Klimova, SBA-15 supports modified by Ti and Zr grafting for NiMo hydrodesulfurization catalysts, Catal. Today 116 (2006) 485–497.

[36] R.G. Nair, J.K. Roy, S.K. Samdarshi, A.K. Mukherjee, Mixed phase V doped titania shows high photoactivity for disinfection of *Escherichia coli* and detoxification of phenol, Sol. Energy Mater. Sol. Cells 105 (2012) 103–108.

[37] M. Benmoussa, E. Ibnouelghazi, A. Bennouna, E. Ameziane, Structural, electrical and optical properties of sputtered vanadium pentoxide thin films, Thin Solid Films 265 (1995) 22–28.

[38] M.A. Larrubia, G. Busca, An ultraviolet–visible-near infrared study of the electronic structure of oxide-supported vanadia–tungsta and vanadia–molybdena, Mater. Chem. Phys. 72 (2001) 337–346.

[39] B.M. Reddy, P.M. Sreekanth, E.P. Reddy, Y. Yamada, Q. Xu, H. Sakurai, T. Kobayashi, Surface characterization of La_2O_3–TiO_2 and V_2O_5/La_2O_3–TiO_2 catalysts, J. Phys. Chem. B 106 (2002) 5695–5700.

[40] N. Yao, S. Cao, K.L. Yeung, Mesoporous TiO_2–SiO_2 aerogels with hierarchal pore structures, Microporous Mesoporous Mater. 117 (2009) 570–579.

[41] G.N. Shao, S.M. Imran, S.J. Jeon, M. Engole, N. Abbas, M. Salman Haider, S.J. Kang, H.T. Kim, Sol–gel synthesis of photoactive zirconia–titania from metal salts and investigation of their photocatalytic properties in the photodegradation of methylene blue, Powder Technol. 258 (2014) 99–109.

[42] A. Hilonga, J.-K. Kim, P. Sarawade, H. Kim, Mesoporous titania–silica composite from sodium silicate and titanium oxychloride. Part I: grafting method, J. Mater. Sci. 45 (2010) 1255–1263.

[43] S. Cao, K.L. Yeung, P.-L. Yue, An investigation of trichloroethylene photocatalytic oxidation on mesoporous titania–silica aerogel catalysts, Appl. Catal. B 76 (2007) 64–72.

[44] S. Cao, K.L. Yeung, J.K.C. Kwan, P.M.T. To, S.C.T. Yu, An investigation of the performance of catalytic aerogel filters, Appl. Catal. B 86 (2009) 127–136.

[45] A. Fujishima, X. Zhang, Titanium dioxide photocatalysis: present situation and future approaches, C. R. Chim. 9 (2006) 750–760.

[46] A. Di Paola, G. Cufalo, M. Addamo, M. Bellardita, R. Campostrini, M. Ischia, R. Ceccato, L. Palmisano, Photocatalytic activity of nanocrystalline TiO_2 (brookite, rutile and brookite-based) powders prepared by thermohydrolysis of $TiCl_4$ in aqueous chloride solutions, Colloids Surf., A 317 (2008) 366–376.

[47] B. Ohtani, Photocatalysis A to Z—what we know and what we do not know in a scientific sense, J. Photochem. Photobiol., C 11 (2010) 157–178.

[48] K. Kusakabe, M. Ezaki, A. Sakoguchi, K. Oda, N. Ikeda, Photocatalytic behaviors of silica-loaded mesoporous titania, Chem. Eng. J. 180 (2012) 245–249.

[49] L. Luo, A.T. Cooper, M. Fan, Preparation and application of nanoglued binary titania–silica aerogel, J. Hazard. Mater. 161 (2009) 175–182.

[50] K. Hashimoto, H. Irie, A. Fujishima, TiO_2 photocatalysis: a historical overview and future prospects, Jpn. J. Appl. Phys. Part 1. Reg. Pap. Short Notes Rev. Pap. 44 (2005) 8269.

[51] M.A. Ahmed, E.E. El-Katori, Z.H. Gharni, Photocatalytic degradation of methylene blue dye using Fe_2O_3/TiO_2 nanoparticles prepared by sol–gel method, J. Alloys Comp. 553 (2013) 19–29.

[52] T. Ohno, K. Sarukawa, M. Matsumura, Photocatalytic activities of pure rutile particles isolated from TiO_2 powder by dissolving the anatase component in HF solution, J. Phys. Chem. B 105 (2001) 2417–2420.